

# Solution of Parabolic Partial Differential Equations in Complex Geometries by a Modified Fourier Collocation Method

Knut S. Eckhoff\*

Carl Erik Wasberg\*

## Abstract

The heat equation with Dirichlet boundary conditions is solved in various geometries by a modified Fourier collocation method. The computational domain is embedded in a larger, regular domain with a uniform, Cartesian grid, and the solution is defined to be identically zero outside the original domain. The discontinuities thus introduced across the boundary are handled by the modified Fourier collocation method, such that highly accurate approximations to the spatial derivatives along each grid line can be calculated. One-dimensional applications are presented to demonstrate the accuracy and the robustness of the method. A detected robustness problem with respect to the location of boundary points relative to grid points is discussed, and modifications that stabilize the method are presented. Two-dimensional problems are then solved with high accuracy, and the flexibility with respect to complex geometries is demonstrated.

**Key words:** spectral methods, Fourier series, Bernoulli polynomials, parabolic partial differential equations, complex geometries.

**AMS subject classifications:** 65M70, 65M20, 35K05.

## 1 Introduction

The modified Fourier collocation method presented in [5] constitutes a flexible scheme which, in principle, is applicable to a large class of initial-boundary value problems for partial differential equations in complex geometries. The

---

\*Dept. of Mathematics, University of Bergen, Allégt. 55, N-5007 Bergen, Norway.

ICOSAHOM'95: Proceedings of the Third International Conference on Spectral and High Order Methods. ©1996 Houston Journal of Mathematics, University of Houston.

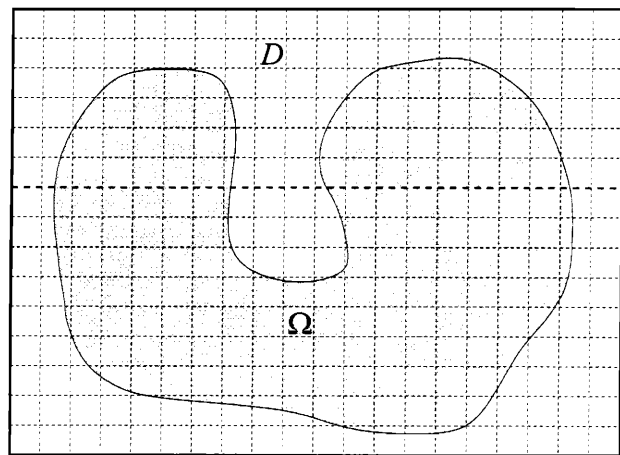


Figure 1: A domain  $\Omega$  with complex geometry embedded in a rectangular domain  $D$ , with a regular grid.

method uses a combination of trigonometric functions and polynomials to represent the functions involved along each grid line. Such representations have previously, to some extent, been considered by Lanczos [9] and others, e.g. [7, 10], in less general contexts.

As a model problem we shall, in this paper, study the heat equation subject to given initial conditions and Dirichlet boundary conditions:

$$(1) \quad \begin{aligned} u_t &= \nabla^2 u, & \mathbf{x} \in \Omega \subset \mathbb{R}^d, & \quad t > 0, \\ u(\mathbf{x}, 0) &= u_0(\mathbf{x}), & \mathbf{x} \in \Omega, \\ u(\mathbf{x}, t) &= g(\mathbf{x}, t), & \mathbf{x} \in \partial\Omega. \end{aligned}$$

Traditional numerical methods for such problems are normally of low order and utilize grids which are adapted to the actual geometry of the problem. When the given domain  $\Omega$  has a complex geometry and high accuracy is desirable, (1) is consequently a challenging problem.

A well-known technique (see e.g. [12]) is to embed the domain  $\Omega$  in a larger, rectangular domain  $D$  with a uniform, Cartesian grid, as shown in figure 1. This approach has

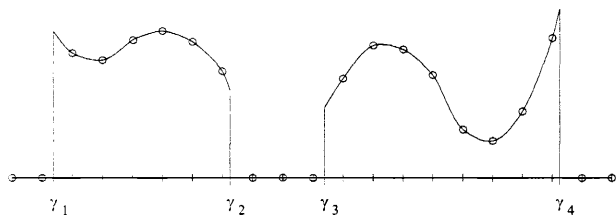


Figure 2: An example of a solution along the grid line marked in figure 1. Circles indicate the values at the grid points, and  $\gamma_1$ – $\gamma_4$  denote the points where the grid line intersects the boundary  $\partial\Omega$ .

been used in various ways, e.g. [2, 11, 13], involving modifications of the governing partial differential equations to account for the boundary conditions. The modified Fourier collocation method described in [5] applies a totally different strategy than earlier approaches. The partial differential equation is not changed and is not solved at grid points outside the original domain. The embedding domain is only used to represent the solution in a way which facilitates the calculation of derivatives.

The grid points inside  $\Omega$  will be referred to as “interior points”, while the rest are called “exterior points”. The solution is defined to be zero at all the exterior points, and the method of lines is applied in order to solve (1) at the interior points.

When the solution  $u(\mathbf{x}, t)$  is given on the uniform grid at a certain instant  $t$ , the spatial derivatives at the grid points can clearly be determined by considering  $u(\mathbf{x}, t)$  along each grid line separately. As an example, the solution  $u(\mathbf{x}, t)$  along the grid line marked in figure 1 may look something like that indicated in figure 2.

One-dimensional functions along each grid line have to be differentiated in our approach, and as illustrated in figure 2, these functions can be expected to be piecewise smooth with jump-singularities at the points stemming from the boundary  $\partial\Omega$ . In section 2 we briefly review the main features of the method presented in [5] for handling the possible discontinuities introduced in the solution or its derivatives at these boundary points. In this connection we note that boundary points do not normally coincide with grid points.

The method is in section 3 applied to the one-dimensional problem (1). In section 4 we discuss robustness problems connected with the location of the boundary points, and show how these problems can be overcome for general geometries. With these modifications, the application of the method presented in [5] to two-dimensional problems (1) is relatively straightforward, and examples are given in section 5. Finally, in section 6, we give some concluding

remarks.

## 2 The modified Fourier collocation method

We shall denote by  $w(x)$  the solution of the problem (1) along an arbitrarily given grid line (in the  $x$ -,  $y$ - or  $z$ -direction) at an arbitrarily given instant  $t$ . Since we clearly, without loss of generality, may take the domain  $D$  to be  $[0, 2\pi]^d$ ; the one-dimensional function  $w(x)$  can be assumed to be a piecewise smooth function defined on the interval  $[0, 2\pi]$ . Following [5], a representation of the solution on the following form is sought:

$$(2) \quad w(x) = w^Q(x) + \sum_{j=1}^M \sum_{n=0}^Q A_j^n V_n(x; \gamma_j).$$

Here the functions  $V_n(x; \gamma_j)$  are determined for  $n = 0, 1, \dots$  by the Bernoulli polynomials  $B_{n+1}(x)$  [1] in the following way:

$$(3) \quad \begin{aligned} V_n(x; \gamma_j) &= -\frac{(2\pi)^n}{(n+1)!} B_{n+1}\left(\frac{x - \gamma_j}{2\pi}\right), \\ & \quad 0 \leq x - \gamma_j \leq 2\pi, \\ V_n(x; \gamma_j) &= V_n(2\pi + x; \gamma_j), \quad -2\pi \leq x - \gamma_j < 0. \end{aligned}$$

In the context of this paper  $\gamma_j$ ,  $j = 1, 2, \dots, M$ , shall denote the points where the boundary  $\partial\Omega$  of the original domain intersects the given grid line.

By definition, the function  $V_n(x; \gamma_j)$  is a piecewise polynomial function of degree  $n + 1$  which is  $n - 1$  times continuously differentiable on  $[0, 2\pi]$ , while the  $n$ th derivative of  $V_n(x; \gamma_j)$  suffers a jump discontinuity of magnitude 1 at  $x = \gamma_j$ . If we for  $n = 0, 1, 2, \dots, Q$ ,  $j = 1, 2, \dots, M$ , let  $A_j^n$  be given as the jump in the  $n$ th derivative of  $w(x)$  at  $x = \gamma_j$ :

$$(4) \quad A_j^n = \frac{d^n w}{dx^n}(\gamma_j^+) - \frac{d^n w}{dx^n}(\gamma_j^-),$$

it readily follows from (2) that the  $2\pi$ -periodic extension of  $w^Q(x)$  is at least  $Q$  times continuously differentiable everywhere. For  $Q$  sufficiently large, the Fourier coefficients associated with  $w^Q(x)$  are therefore rapidly decreasing; and consequently  $w^Q(x)$  can, in this case, be accurately approximated by a truncated Fourier series expansion:

$$(5) \quad w^Q(x) \approx \sum_{k=-N/2+1}^{N/2-1} \hat{w}_k^Q e^{ikx}.$$

Since  $w(x) = 0$  at all exterior points and Dirichlet boundary conditions are assumed, the jumps  $A_j^0$ ,  $j =$

$1, 2, \dots, M$ , can be readily determined by the data given in (1). We subtract the corresponding terms in the following way:

$$(6) \quad w^0(x) = w(x) - \sum_{j=1}^M A_j^0 V_0(x; \gamma_j).$$

Based on the values of this function  $w^0(x)$  at the  $N$  grid points  $x_l = 2\pi l/N$ ,  $l = 0, 1, \dots, N-1$ , we now calculate the corresponding discrete Fourier coefficients  $\tilde{w}_k^0$ .

Still following [5], the jumps  $A_j^n$  in the derivatives up to order  $Q$  are approximately determined as the least squares solution of the overdetermined system

$$(7) \quad \sum_{n=1}^Q \sum_{j=1}^M (\tilde{V}_n)_k(\gamma_j) A_j^n = \tilde{w}_k^0, \\ |k| = N/2 - MQ, \dots, N/2 - 1,$$

where  $(\tilde{V}_n)_k(\gamma_j)$  denote the discrete Fourier coefficients associated with the functions  $V_n(x; \gamma_j)$ . The Fourier coefficients in (5) are then approximately calculated by

$$(8) \quad \hat{w}_k^Q = \tilde{w}_k^0 - \sum_{j=1}^M \sum_{n=1}^Q (\tilde{V}_n)_k(\gamma_j) A_j^n, \\ k = 0, \pm 1, \dots, \pm(N/2 - 1).$$

More details on the calculation of approximate jumps and coefficients can be found in [6].

From (3) and properties of the Bernoulli polynomials, we have for  $x \neq \gamma$ :

$$(9) \quad \frac{d}{dx} V_n(x; \gamma) = V_{n-1}(x; \gamma), \quad n = 1, 2, \dots, \\ \frac{d}{dx} V_0(x; \gamma) = -1/2\pi.$$

The derivatives of  $w(x)$  can therefore be approximately calculated from (2) and (5) when  $x \neq \gamma_j$ ,  $j = 1, \dots, M$ :

$$(10) \quad \frac{d^p w(x)}{dx^p} = \sum_{k=-N/2+1}^{N/2-1} (ik)^p \hat{w}_k^Q e^{ikx} - \frac{1}{2\pi} \sum_{j=1}^M A_j^{p-1} \\ + \sum_{j=1}^M \sum_{n=p}^Q A_j^n V_{n-p}(x; \gamma_j).$$

It is shown in [4, 5] that this method gives a  $(Q+1-p)$ 'th order accurate approximation to the  $p$ th derivative of  $w(x)$  for  $p = 0, 1, \dots, Q$ , when  $N \rightarrow \infty$ . We also note that formal spectral accuracy can here, in principle, be obtained by defining the parameter  $Q$  as a function of  $N$ .

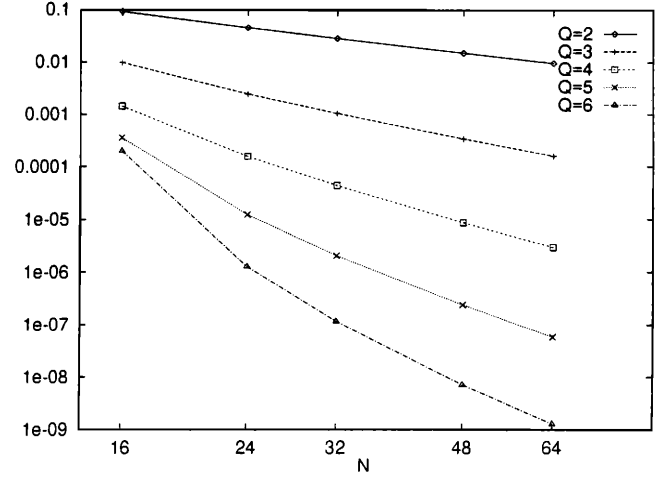


Figure 3: RMS-error over the grid points for the approximate second derivative of the function (11).

$Q$	2	3	4	5	6
Theoretically expected order	1.5	2.5	3.5	4.5	5.5
Experimental order	1.6	2.7	3.9	5.2	6.5

Table 1: Convergence orders for the RMS-error of the approximation to the second derivative of the function (11).

To demonstrate the order estimates numerically, we consider as an example the accuracy of the calculated second derivative of the following function:

$$(11) \quad u(x) = -\exp(x/2) + (\exp(\pi) - 1)x/2\pi + 1, \\ 0 \leq x \leq 2\pi.$$

The RMS-errors are shown in figure 3. With the exception of the smallest values of  $N$  for  $Q = 5$  and  $Q = 6$ , the curves of the maximum errors in figure 3 are close to straight lines, as expected from the asymptotic theory. Approximate orders of convergence found from the slopes of the curves between  $N = 32$  and  $N = 64$ , and are shown in table 1 for different values of  $Q$ . Assuming that the largest errors only occur at the points closest to the boundary points, the RMS-error is expected to be one half order better than the maximum error. These theoretical estimates are given in table 1, and are clearly confirmed by the numerical results.

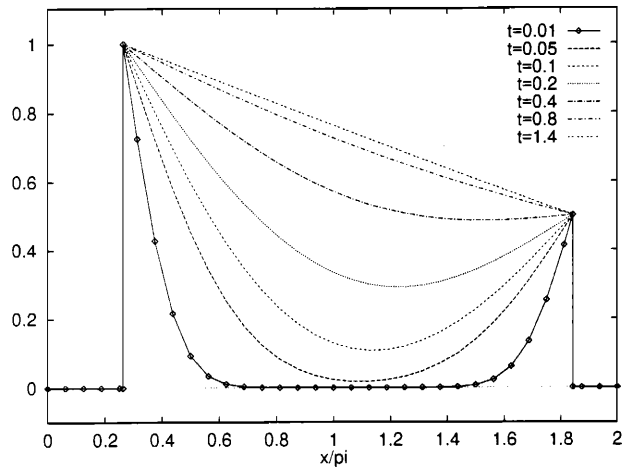


Figure 4: The solution of (12), (13) at different times, calculated with  $N = 32$  and  $Q = 4$ . The positions of the grid points and the two boundary points are shown on the curve for  $t = 0.01$ .

### 3 The heat equation in one dimension

In this section we consider the one-dimensional version of (1), and restrict ourselves to two boundary points ( $M = 2$  in the notation of the previous section):

$$(12) \quad \begin{aligned} u_t &= u_{xx}, & 0 < \gamma_1 < x < \gamma_2 < 2\pi, & \quad t > 0, \\ u(x, 0) &= u_0(x), & 0 < \gamma_1 < x < \gamma_2 < 2\pi, & \\ u(\gamma_1, t) &= g_1(t), & u(\gamma_2, t) = g_2(t), & \quad t > 0. \end{aligned}$$

We want to apply the method described in the previous section for calculating  $u_{xx}$  at each interior grid point (for  $x \in (\gamma_1, \gamma_2)$ ), and solve the resulting system of ordinary differential equations by a fourth order explicit Runge-Kutta method [8].

We first consider (12) with the following initial- and boundary conditions:

$$(13) \quad u_0(x) = 0.0, \quad g_1 = 1.0, \quad g_2 = 0.5.$$

The boundary points are chosen to be

$$(14) \quad \gamma_1 = 0.26\pi, \quad \gamma_2 = 1.84\pi,$$

and the solution at different times for  $N = 32$  and  $Q = 4$  converges nicely to a straight line, as shown in figure 4.

In this example all eigenfunctions associated with the spatial operator in (12) are excited through the incompatibility between the initial- and boundary conditions (13).

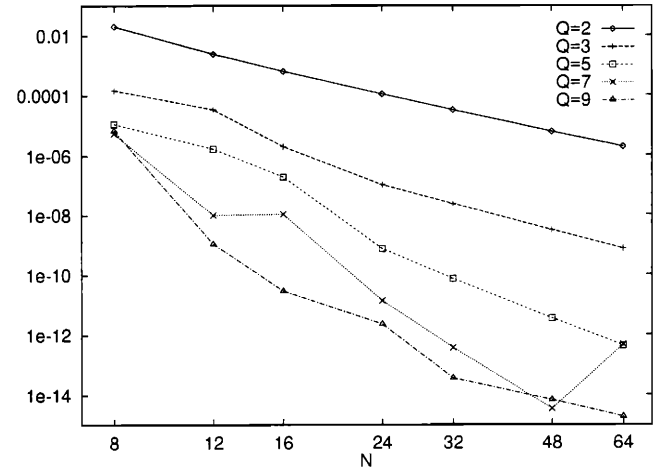


Figure 5: RMS-error at  $t = 0.6$  in the solution of (12), (15).

In order to study the accuracy of the method, it is more revealing to look at the accuracy obtained for the solution of (12) corresponding to the lowest order eigenfunction. In fact, that solution decays more slowly than all other solutions and will; therefore, normally dominate the accuracy.

As will be discussed in section 4, the location of the boundary points relative to the grid points may influence both the approximation accuracy [6] and the stability of the described algorithm for the time-dependent problem (12). To eliminate these effects in the measurement of accuracy, the next example is defined on the full interval  $[0, 2\pi]$ . This means that  $\gamma_1 = 0$ , and  $\gamma_2 = 2\pi$  is identified with  $\gamma_1$  through the periodicity of the representation (2). The initial function, corresponding to the fundamental eigenfunction associated with (12) is then

$$(15) \quad u_0 = \sin(x/2), \quad 0 \leq x \leq 2\pi.$$

With this initial function, the exact solution of (12) at later times is just a scaled version of (15). After integration to  $t = 0.6$ , the solution has decayed to around 10% of the initial function. The RMS-errors at  $t = 0.6$  for different values of  $N$  and  $Q$  are shown in figure 5.

Figure 5 illustrates how the order of accuracy increases with increasing  $Q$ , but it also shows that remarkably good results can be obtained on coarse grids, i.e., far from the asymptotic range where the theoretical error estimates are valid. For the highest values of  $Q$  and  $N$ , the applied numerical precision is the most important limiting factor for the obtained accuracy.

The stability limit for the time-steps was, in our calculations, found to be  $\Delta t \approx 2/N^{2.1}$ , and was virtually inde-

pendent of  $Q$ . The stability limit is, therefore, comparable with the stability limit for the standard Fourier method for periodic problems and considerably better than the  $O(N^{-4})$  limit for Chebyshev or Legendre methods [3] for the problem (12), (15). Even though it would be interesting to search for efficient implicit solvers for the modified Fourier method, these results means that explicit time integration for second order equations is not necessarily prohibitively expensive with this method. We shall therefore, in this work, restrict our attention to explicit methods.

## 4 Discussion of robustness

It was demonstrated in the previous section that the differentiation method described in section 2 produces a stable method for the solution of the one-dimensional heat equation. However, as already mentioned, the stability is found to be sensitive to the location of the boundary points. There are no stability problems when the boundary points coincide with grid points, but for applications to problems in higher dimensions with domains of complex geometry, it is apparent from figure 1 that boundary points at general locations relative to the grid points must normally be dealt with.

In the one-dimensional case it seems that  $Q = 2$  always produces a stable algorithm, while we have observed instabilities in certain circumstances for all higher values of  $Q$ . Apparently, even values of  $Q$  are more robust than odd values, and higher even values of  $Q$  seem less robust than lower ones. For  $Q$  even, it appears that a sufficient condition for stability is that each boundary point is situated at a distance from an *exterior* grid point which is not larger than  $0.6 \cdot \Delta x$ , where  $\Delta x = 2\pi/N$  is the grid spacing.

To at least partially explain this instability, we note that the Dirichlet boundary conditions are introduced only by specifying the jumps in the function values at the boundary points, and subtracting their contributions as described by (6). However, specifying the jump does not introduce a strict control on each of the two one-sided limit values at the boundary point, because the solution at the boundary could in principle then “float”, with correct jump but wrong values. The value of the solution is specified at the exterior grid points, but if the distance from the nearest of these to the boundary point is too large, the “floating” may produce an instability.

One way to avoid the instability may be to adjust the boundary of the domain in such a way that the boundary points on each grid line in each spatial direction are moved to nearby “stable” positions. Since each boundary point only has to be moved within a single grid interval, this

process will clearly converge, but will probably reduce the order of the method. Thus other approaches should be investigated, and this is the topic of the present section.

In the situation considered here, we assume that there is an exterior interval where the solution is identically zero at one side of each boundary point. This information can be used in different ways, and we shall first consider the use of Taylor expansions around the boundary points.

For the case  $M = 2$  we know that

$$(16) \quad \frac{d^n w}{dx^n}(\gamma_1^-) = \frac{d^n w}{dx^n}(\gamma_2^+) = 0, \quad n = 0, 1, 2, \dots$$

The jumps  $A_1^n, A_2^n$  calculated by (7) are known to approximately satisfy (4), hence equation (16) implies that the calculated value of  $A_1^n$  approximates  $w^{(n)}(x)$  at  $x = \gamma_1^+$  and  $-A_2^n$  approximates  $w^{(n)}(x)$  at  $x = \gamma_2^-$ . Since it was shown in [5] that the error in the jump  $A_j^n$  calculated by (7) actually is of the order  $O(N^{-(Q+1-n)})$  as  $N \rightarrow \infty$ , we get that the following approximate Taylor expansion around  $x = \gamma_1$  holds for  $w(x)$  as long as  $0 \leq x - \gamma_1 \leq 2\pi/N$ :

$$(17) \quad w(x) = A_1^0 + (x - \gamma_1)A_1^1 + \frac{(x - \gamma_1)^2}{2!}A_1^2 + \dots \\ + \frac{(x - \gamma_1)^Q}{Q!}A_1^Q + O(N^{-(Q+1)}).$$

A corresponding formula holds for  $0 \leq \gamma_2 - x \leq 2\pi/N$ , except for a change of sign. If  $x_{k-1} \leq \gamma_1 < x_k$  and  $x_l < \gamma_2 \leq x_{l+1}$ , we therefore obtain the following approximate formulas for the second derivative of  $w(x)$  at the interior grid points  $x = x_k$  and  $x = x_l$ :

$$(18) \quad w_{xx}(x_k) = A_1^2 + (x_k - \gamma_1)A_1^3 + \dots + \frac{(x_k - \gamma_1)^{Q-2}}{(Q-2)!}A_1^Q, \\ w_{xx}(x_l) = -A_2^2 - (x_l - \gamma_2)A_2^3 - \dots - \frac{(x_l - \gamma_2)^{Q-2}}{(Q-2)!}A_2^Q.$$

With this modification introduced, we have not detected instabilities when  $Q$  is even. Although unstable situations have been observed in some cases for odd values of  $Q$ , the modification has been seen to have a stabilizing effect for most cases.

Unfortunately, however, calculations show that the accuracy of the calculated second derivative normally decreases at the grid points where the Taylor expansion method (18) is applied, even though the formal approximation error is of the same order as in the original method. We shall therefore consider another approach, which also has more general applications [4].

From (2) and the corresponding discrete Fourier series

$$I_N w(x) = I_N w^Q(x) + \sum_{j=1}^M \sum_{n=0}^Q A_j^n I_N V_n(x; \gamma_j),$$

the following equations can be derived for  $m = 0, 1, 2, \dots$  as  $N \rightarrow \infty$ :

$$(19) \quad \sum_{n=0}^Q \sum_{j=1}^M \left( \frac{d^m}{dx^m} V_n(x; \gamma_j) - \frac{d^m}{dx^m} I_N V_n(x; \gamma_j) \right) A_j^n - \frac{d^m}{dx^m} w(x) + \frac{d^m}{dx^m} I_N w(x) = O(N^{-(Q+1-m)}).$$

For  $x$  anywhere in the exterior intervals, the term  $\frac{d^m}{dx^m} w(x)$  is zero, so the only unknowns in (19) are the jumps  $A_j^n$  for  $n = 1, 2, \dots$ , and  $j = 1, 2, \dots, M$ . It can be shown [4] that the error in  $A_j^n$  calculated from (19) is of the same order when  $N \rightarrow \infty$  as for the jumps calculated by the spectral equations (7).

Following the comments made earlier in this section about “floating” boundary values, it is natural to evaluate (19) at the limits as  $x \rightarrow \gamma_j$  from the outside, i.e., from an exterior interval. Numerical experiments have shown that if (19) with  $m = 0, 1, 2$  are added to the system of equations (7), we obtain stable calculations regardless of the boundary locations.

There is a price to pay for including the additional equations (19) in the calculations of the jumps, however, namely that the second derivative operator may become more stiff, manifested through a negative eigenvalue with large magnitude. This occurs in the same situations which previously led to instabilities; when a boundary point is located close to an interior grid point. Thus, stable calculations require shorter time-steps for explicit time-integration in such cases.

An illustration is given in figure 6, where the absolute value of the largest negative eigenvalue of the second derivative operator is plotted for  $N = 32$  and  $Q = 4$ . The right boundary point  $\gamma_2$  is fixed at  $29.5\Delta x$ , while the position of the left boundary point  $\gamma_1$  varies, and it is clearly seen that positions close to interior grid points lead to growth in the eigenvalue. This growth has been found to be largest when (19) is used with  $m = 0$  only, and decreases when higher values of  $m$  are used, but only small improvements are achieved by using values of  $m$  larger than 2.

Even in the worst cases displayed in figure 6, the eigenvalue is only increased by a factor of about 10. As this is still small compared to  $N^2$ , it does not seriously affect the comments made in the previous section about explicit time-integration. However, there is clearly a potential gain if this growth can be avoided, because some boundary points must be expected to end up close to the least favorable positions when problems in complex geometries in higher dimensions are solved. We hope in the near future to be able to describe such improvements elsewhere.

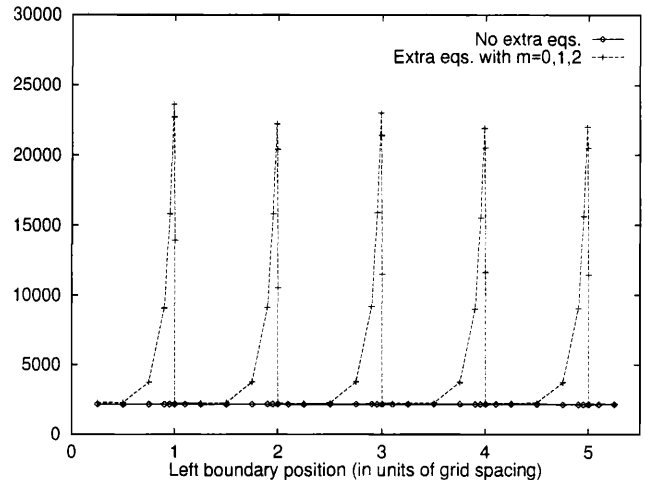


Figure 6: Magnitude of the negative eigenvalue with largest absolute value for the second derivative operator with Dirichlet boundary conditions, as a function of the position  $\gamma_1$  of the left boundary point for  $N = 32$ ,  $Q = 4$ ,  $\gamma_2 = 29.5\Delta x$ .

## 5 The heat equation in two dimensions

In this section we consider the two-dimensional version of (1):

$$(20) \quad \begin{aligned} u_t &= u_{xx} + u_{yy}, & (x, y) \in \Omega, & \quad t > 0, \\ u(x, y, 0) &= u_0(x, y), & (x, y) \in \Omega, \\ u(x, y, t) &= g(x, y), & (x, y) \in \partial\Omega. \end{aligned}$$

Compared to the solution method for the one-dimensional case in section 3, the only change in the procedure needed here is that the derivatives must be calculated along every grid line in both the spatial directions. The shape of the domain  $\Omega$  will clearly, in general, give different locations for the boundary points for each such grid line.

We shall first study an example where the exact solution is easy to obtain, namely the case where  $\Omega$  is a circular domain with centre at  $(x_0, y_0)$  and radius  $r_0$ :

$$(21) \quad \begin{aligned} \Omega &= \{(x, y) | (x - x_0)^2 + (y - y_0)^2 < r_0^2\}, \\ x_0 &= 1.1\pi, \quad y_0 = 0.95\pi, \quad r_0 = 0.75\pi. \end{aligned}$$

Corresponding to the one-dimensional example (12), (15), we choose the initial condition to be the most slowly decaying eigenfunction for the spatial operator in (20) on the domain (21):

$$(22) \quad u_0(x, y) = J_0 \left( \lambda_1 \sqrt{(x - x_0)^2 + (y - y_0)^2} / r_0 \right).$$

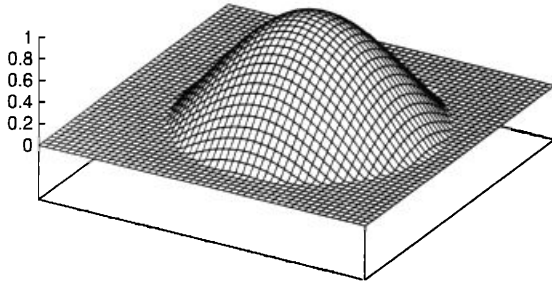


Figure 7: The initial condition (22) on the circle (21), shown on a  $48 \times 48$  grid.

Here  $J_0$  is the Bessel function of the first kind of order zero, and  $\lambda_1 \approx 2.40$  is its first zero [1]. A homogeneous boundary condition is applied:

$$(23) \quad g(x, y) = 0, \quad \text{when} \quad (x - x_0)^2 + (y - y_0)^2 = r_0^2.$$

The initial condition (22) is shown in figure 7, and the solution at  $t = 0.05$ , calculated with  $N_x = N_y = 48$  and  $Q = 6$ , is shown in figure 8.

Figure 9 shows the RMS-error at  $t = 0.05$  for different values of  $N_x = N_y = N$  and  $Q$ . The exact solution at  $t = 0.05$  is equal to the initial condition multiplied by a scaling factor 0.60. These results were obtained when the additional equations (19) with  $m = 0, 1, 2$  were included at the exterior limits of the boundary points. As for the one-dimensional results in figure 5, the convergence is algebraic when the number of grid points are large enough, but we note that quite accurate results are obtained also on the coarser grids.

Finally, we want to demonstrate the flexibility of the method with regard to more complex geometries. The considered domain is shown in figure 10, and the initial- and boundary conditions are chosen as

$$(24) \quad \begin{aligned} u_0(x, y) &= 0.08 + 0.23(1 + \cos(x - 0.8\pi)) \\ &\quad (1 + \cos(y - 0.9\pi)), \quad (x, y) \in \Omega, \\ g(x, y, t) &= u_0(x, y), \quad (x, y) \in \partial\Omega, \end{aligned}$$

and displayed in figure 11. To calculate the solution for this problem, the only necessary modifications of the program used in the previous example are to adjust the parameters

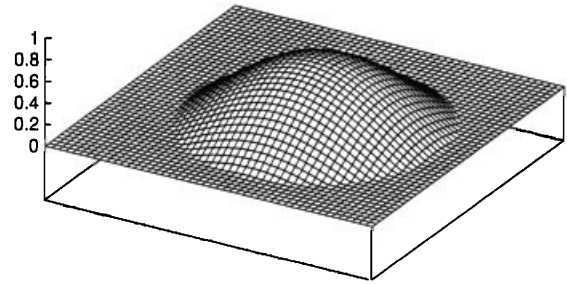


Figure 8: Solution at  $t = 0.05$  of the two-dimensional heat equation (20) on the circle (21) with the initial condition (22), calculated with  $N_x = N_y = 48$  and  $Q = 6$ .

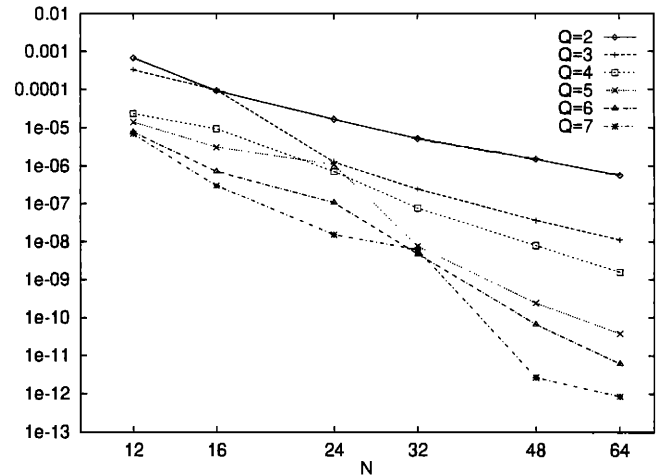


Figure 9: RMS error of solutions at  $t = 0.05$  of the two-dimensional heat equation on the circle (21), with the initial condition (22).

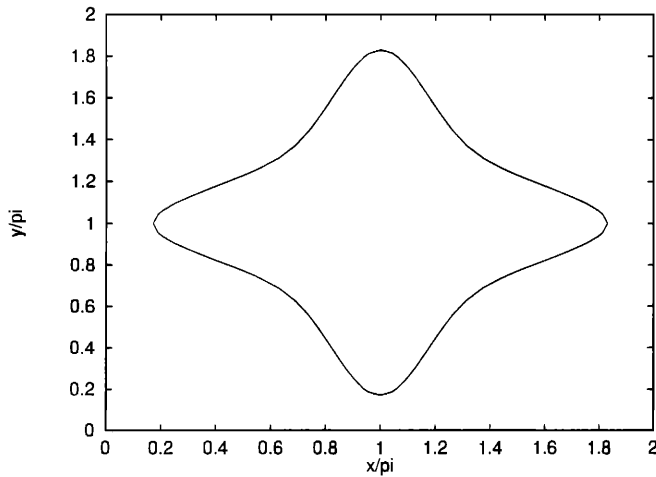


Figure 10: The boundary of the domain used in the final example.

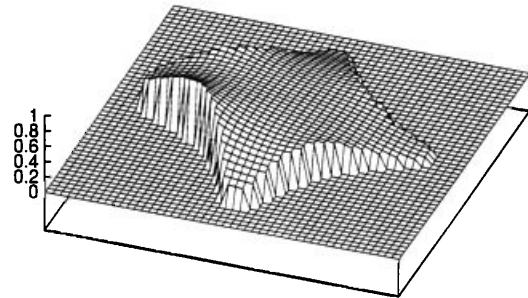


Figure 12: Solution at  $t = 0.2$  of the two-dimensional heat equation (20) on the domain shown in figure 10 and with the initial- and boundary conditions (24), calculated with  $N_x = N_y = 48$  and  $Q = 4$ .

$\gamma_1, \gamma_2$  for each grid line to the new locations of the boundary points, and give the corresponding jumps deduced from the Dirichlet boundary conditions.

The solution at  $t = 0.2$ , calculated with  $N_x = N_y = 48$  and  $Q = 4$  is shown in figure 12. This is practically the steady-state solution, i.e., the solution of the Dirichlet problem for the Laplace equation on the given domain.

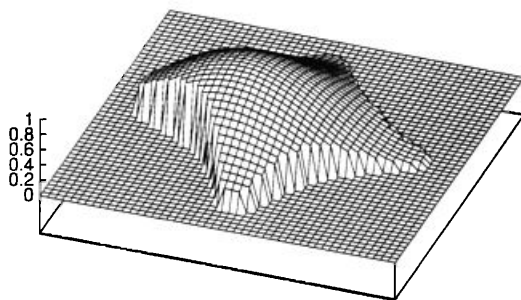


Figure 11: The initial condition (24) on the domain from figure 10, shown on a  $48 \times 48$  grid.

## 6 Conclusions

The modified Fourier collocation method [5] has been applied to the solution of the heat equation with Dirichlet boundary conditions on various domains in one and two spatial dimensions. Highly accurate solutions of test problems have been obtained with uniform, Cartesian grids of typically 32–64 points in each direction. The method is, in principle, flexible with respect to the geometry of the computational domain; but turns out to be sensitive to the location of boundary points relative to the grid points. Various ways of eliminating this sensitivity by incorporating additional available information at the boundaries have been discussed.

The most attractive feature of the method lies in the ease with which different geometries are implemented; combined with the high orders of accuracy obtained.

## References

- [1] M. Abramowitz and I. A. Stegun. *Handbook of Mathematical Functions*. Dover, New York, 1970.
- [2] B. L. Buzbee, F. W. Dorr, J. A. George, and G. H. Golub. The direct solution of the discrete Poisson equation on irregular regions. *SIAM J. Numer. Anal.*, 8:722–736, 1971.
- [3] C. Canuto, M. Y. Hussaini, A. Quarteroni, and T. A. Zang. *Spectral methods in fluid dynamics*. Springer-Verlag, New York, 1988.
- [4] K. S. Eckhoff. On a high order numerical method for functions with singularities. In preparation, 1995.
- [5] K. S. Eckhoff. On a high order numerical method for solving partial differential equations in complex geometries. To appear in *J. Sci. Comput.*, 1995.
- [6] K. S. Eckhoff and C. E. Wasberg. On the numerical approximation of derivatives by a modified Fourier collocation method. Technical Report No. 99, Dept. of Mathematics, University of Bergen, Allégt. 55, N-5007 Bergen, Norway, July 1995.
- [7] D. Gottlieb and S. A. Orszag. *Numerical analysis of spectral methods: Theory and applications*. SIAM, Philadelphia, 1977.
- [8] E. Hairer, S. P. Nørsett, and G. Wanner. *Solving ordinary differential equations I, Nonstiff problems*. Springer-Verlag, New York, 1987.
- [9] C. Lanczos. *Discourse on Fourier Series*. Hafner, New York, 1966.
- [10] J. N. Lyness. Computational techniques based on the Lanczos representation. *Math. Comp.*, 28:81–123, 1974.
- [11] C. S. Peskin. Flow patterns around heart valves: A numerical method. *J. Comput. Phys.*, 10:252–271, 1972.
- [12] G. D. Smith. *Numerical Solution of Partial Differential Equations: Finite Difference Methods*. Oxford University Press, Oxford, 1965.
- [13] J. A. Viecelli. A method for including arbitrary external boundaries in the MAC incompressible fluid computing technique. *J. Comput. Phys.*, 4:543–551, 1969.

